ELSEVIER

Thermochimica Acta 330 (1999) 109–119

thermochimica acta

Advanced AC calorimetry of polycaprolactone in melting region

A.A. Minakov[a,*], C. Schick[b]

[a]*General Physics Institute, R.A.S., Vavilov st. 38, 117942, Moscow, Russian Federation*
[b]*Department of Physics, University of Rostock, Universitatsplatz 3, 18051 Rostock, Germany*

Received 13 August 1998; accepted 23 December 1998

Abstract

The new capabilities of AC calorimetry, when working at frequencies above the classical limit were demonstrated. The appropriate frequency range of classical AC calorimetry was substantially enlarged. It was shown that the advanced AC calorimetry can be applied for studying dynamic heat capacity of polymers in the frequency range 0.1–1 Hz. Thus, the processes with characteristic time as short as ca. 5 s was registered. The advanced AC technique was applied for investigation of the melting kinetics in polycaprolactone. It was found that melting in polycaprolactone is related to an activated process. The activation of the melting process after a step heating is described by a stretched exponent and the decay of the melting by only one exponent at short times. The dependencies of the exponent on temperature and thermal treatment were investigated at frequencies in the range 0.1–1Hz and modulation amplitudes 0.005–0.2 K.

Keywords: AC calorimetry; Dynamic heat capacity; Thermal conductivity; Melting kinetics; Polymers

1. Introduction

AC calorimetry is a powerful technique, which was successfully used for dynamic heat capacity measurements in micro-samples of inorganic materials [1–5]. Investigation of dynamic heat capacity in polymers could provide a unique information about relaxation phenomena, crystallization and melting kinetics in these materials. This is important for understanding their physics, as well as for providing practically valuable information. The melting kinetics of polymers is investigated insufficiently, because melting process in polymers is often as fast as the conduction of heat of fusion into the sample [6]. Thus, it is extremely important to investigate micro-samples. The AC calorimetry could provide this unique possibility. However, the thermal conductivity of the polymers is so small, that only in millihertz frequency range the classical AC calorimetry can be applied correctly to polymers [7], as well as other modulation techniques, such as temperature-modulated differential scanning calorimetry, TMDSC [8]. Obviously, the shortest possible apparatus time lag is of the order of inverse frequency, because at least one period of oscillations is necessary for signal detection. Thus, only the slow processes can be investigated at low frequencies [9]. For this reason, the melting kinetics of polymers is not investigated in such detail as the crystallization process, which is usually slow enough to be studied [6]. The width of appropriate frequency range of the classical AC calorimetry can be substantially enlarged, as proved recently [10]. It was shown that the advanced AC calorimetry can be successfully

*Corresponding author. Fax: +7-095-135-82-81; e-mail: minakov@ran.gpi.ru

0040-6031/99/$ – see front matter
PII: S0040-6031(99)00025-8

applied to study the dynamic heat capacity of polymers at frequencies up to ca. 1 Hz. Thus, the processes with characteristic time as short as ca. 1 s can be registered.

The focus of this paper is to demonstrate how the advanced AC technique can be applied for the investigation of melting kinetics in polymers. We aim to show the capabilities of AC calorimetry, when working at frequencies above the classical limit. In this regime, information on sample properties can be obtained by measuring phase and amplitude of sample temperature modulation. Heat capacity and thermal conductivity can be determined simultaneously. Further, we present experimental data obtained for polycaprolactone (PCL), in order to illustrate the capabilities of the technique. New information about melting kinetics of this material is presented.

2. Experimental

2.1. Method

The experiments were carried out with the AC calorimeter described in [10]. The calorimeter cell – the system for creation and registration of temperature modulation in a disk-shaped sample – consists of a heater, a sensor, and a holder. The sample is placed between the heater and the sensor substrates. The heat contact between the sample and substrates was very good after the first sample melting due to nice adhesion of PCL to the substrates. The heater and the sensor are formed on the surfaces of the polished sapphire disks of 3 mm diameter and of thickness d_0=0.1 mm. The heater is a chromium film ca. 0.1 μm, sputtered on the first sapphire substrate. Copper contact pads are sputtered on the film, and copper wires of 0.05 mm diameter are welded to the pads. The resistance of the film after special thermal treatment is stable during five years and equals 100±10 Ω over the temperature range 4.2–400 K. The power of the resistive heater equals $P_0(1+\cos \omega t)$, where $\omega/2$ is the angular frequency of the electric current and P_0 is the average power of the heater. To form the sensor, a copper field is sputtered on the second sapphire substrate. The thermocouple (Cu–Cu:Fe) microwires of 0.05 mm diameter are welded to the copper field. The sensitivity of the thermocouple is about 0.01 mV/K in the range 1–400 K. The sensor is glued on a silk net, which serves as holder. Thus, the system consists of four layers, including the sample.

The system is heated by uniform heat flow of oscillating rate $P=P_0 \cos(\omega t)$. The flow is applied to the outer face of the first layer at $z=0$ and propagates through the layered system along z-axis. The cross area S of the system is independent on z. Provided the heat leakage through the perimeter of the system is negligible, the plane temperature waves $T=\mathrm{Re}[T_0 \exp(\mathrm{i}\omega t \pm \mathbf{k}z)]$ *propagate across the system, where* $\mathbf{k}=\exp(\mathrm{i}\pi/4)(\omega c/\kappa)^{1/2}$, c – specific heat capacity and κ – thermal conductivity of the material. In other words $\mathbf{k} = (k + ik)/\sqrt{2}$, where mod($\mathbf{k}$) equals $k = \sqrt{\omega c/\kappa}$. Thus, the wave number and the damping coefficient of these waves are equal to $k/\sqrt{2}$. Stationary oscillating solution of the heat transfer equation without heat sources can be written as follows: $\mathrm{Re}\{\exp(i\omega t)\,[\mathbf{a}\sinh(\mathbf{k}z) + \mathbf{b}\cosh(\mathbf{k}z)]\}$. Therefore the temperature wave $\mathbf{T}_i(z) = \exp(i\omega t)\ \mathbf{a}_i \sinh[\mathbf{k}_i(z-\xi_i)] + \mathbf{b}_i \cosh[\mathbf{k}_i(z-\xi_i)]\}$ is excited in ith layer, where ξ_i is the coordinate of ith boundary. The complex coefficients $\mathbf{a}_i$ and $\mathbf{b}_i$ are determined by the boundary conditions for temperature and heat flow amplitudes on faces of ith layer. The amplitude $\mathbf{T}_\mathrm{A}$ of the temperature modulation is measured on the surface between the sensor and the holder. Thus, the amplitude and the phase of the temperature wave propagating though the sample is measured. This method can be therefore named as *Temperature–Waves–Transmission Spectroscopy.*

In classical AC calorimetry one measures the effective heat capacity

$$\mathbf{C}_\mathrm{eff} = P_0/(i\omega \mathbf{T}_A), \tag{1}$$

which is proportional to the heat-flow amplitude P_0 and inversely proportional to the complex amplitude $\mathbf{T}_\mathrm{A}$. Of course, at sufficiently low frequencies and sufficiently low heat-link between the system and the thermostat the effective heat capacity $\mathbf{C}_\mathrm{eff}$ equals the sum of the sample heat capacity C_s and the heat capacity of the empty cell. The phase shift $\varphi = -\mathrm{Arg}\,(\mathbf{C}_\mathrm{eff})$ between the temperature modulations in the heater and in the sensor equals to zero at these conditions. It is noteworthy that, the phase shift between the heat-flow and $\mathbf{T}_\mathrm{A}$ equals $\varphi - \pi/2$. As the trivial phase lag $\pi/2$ is not of interest, we consider the

phase shift φ between temperature modulations on the opposite sides of the system. At higher frequencies, as it was shown in [10], the measured value $\mathbf{C}_{\rm eff}$ for the Heater–Sample–Sensor–Holder system can be expressed as follows:

$$\mathbf{C}_{\rm eff} = \cosh(\boldsymbol{\alpha}_0)\cosh(\boldsymbol{\alpha}_{\rm s})\exp(-{\rm i}\pi/4) \times [\mathbf{A} + \gamma_{\rm s}\tanh(\boldsymbol{\alpha}_{\rm s}) + \mathbf{B}]\,\mathbf{F}, \quad (2)$$

$$\mathbf{A} = C_0\tanh(\boldsymbol{\alpha}_0)/\alpha_0 + C_{\rm h}\tanh(\boldsymbol{\alpha}_{\rm h})/\alpha_{\rm h} + (1-i)\Gamma/f,$$

where $\boldsymbol{\alpha}_i = \exp({\rm i}\pi/4)\,d_i\,(\omega c_i/\kappa_i)^{1/2}$ – the parameter characterizing the thermal length of the ith layer, d_i is the thickness of the ith layer, $C_{\rm h}$, $\boldsymbol{\alpha}_{\rm h}$, $C_{\rm s}$, $\boldsymbol{\alpha}_{\rm s}$ and C_0, $\boldsymbol{\alpha}_0$ – the corresponding parameters of holder, sample and two sapphire substrates of the heater and the sensor, respectively, Γ – the constant, depending on the heat-link between the system and the thermostat, $f=\omega/2\pi$ – the frequency of the temperature modulation, and $\gamma_{\rm s}=C_{\rm s}/\alpha_{\rm s}$. The cross terms are presented by the sum $\mathbf{B} = \mathbf{B}_3 + \mathbf{B}_5 + \cdots + \mathbf{B}_{2m+1}$, where $2m+1 \le n$. Denote $\beta_{ab} = \kappa_a k_a/\kappa_b k_b$, then $\mathbf{B}_{\rm i}$ can be written as follows:

$$\mathbf{B}_3 = \sum (C_a/\alpha_a\,\beta_{cb}\tanh(\boldsymbol{\alpha}_a)\tanh(\boldsymbol{\alpha}_b)\tanh(\boldsymbol{\alpha}_c), \quad (3)$$

$$\mathbf{B}_5 = \sum (C_a/\alpha_a)\,\beta_{cb}\,\beta_{ed}\tanh(\boldsymbol{\alpha}_a)\tanh(\boldsymbol{\alpha}_b)\tanh(\boldsymbol{\alpha}_c)\tanh(\boldsymbol{\alpha}_d)\tanh(\boldsymbol{\alpha}_e),$$

and so on for all indexes, such as $a<b<c<d<e\ldots$. The sum $\mathbf{B}_3$ is taken over all combinations of three elements from n, $\mathbf{B}_5$ – over all combinations of five elements from n, and so on. The cross terms are negligibly small at sufficiently low frequencies. Indeed, $\mathrm{th}(\boldsymbol{\alpha}_i)\approx\boldsymbol{\alpha}_i$ *at small* α_i*, and* α_i *decrease with frequency as* $\alpha_i \sim \sqrt{\omega}$*. The coefficient* $\mathbf{F}$ describes the heat leakage into the wires of the thermocouple. At frequencies not too high the coefficient $\mathbf{F}$ can be substituted by 1. This is only the parameter Γ depends on ambient gas pressure. But this dependence is very weak in the pressure range 1–100 Pa. In all measurements the pressure of helium gas was ca. 10 Pa. The parameters α_0, $\alpha_{\rm h}$, C_0, $C_{\rm h}$ and Γ was determined in advance without a sample. Then, the two coefficients $\gamma_{\rm s}$ and $\alpha_{\rm s}$ can be calculated from the two measured values, $\mathrm{Re}\mathbf{C}_{\rm eff}$ and $\mathrm{Im}\mathbf{C}_{\rm eff}$, using Eq. (2). Finally, the sample heat capacity and thermal conductivity can be expressed as follows:

$$C_{\rm s} = \gamma_{\rm s}\,\alpha_{\rm s}, \quad (4)$$
$$\kappa_{\rm s} = \omega d_{\rm s}\gamma_{\rm s}/S\alpha_{\rm s}.$$

It is noteworthy that, when the results are presented in this form, the accuracy of the measured sample heat capacity is independent on the errors of the measurements of the sample face area S and thickness $d_{\rm s}$. This is especially important when the sample dimensions are changed during the experiment, e.g., due to thermal expansion. Once the cell calibration is performed, the calibration table is stored in the computer memory. The software that drives the calorimeter uses this table for calculation of the sample parameters $C_{\rm s}$ and $\kappa_{\rm s}$ from the measured values of $C_{\rm eff}$ and the phase shift φ. Thus, the described algorithm makes it possible to carry out simultaneous measurements of heat capacity and thermal conductivity.

2.2. *What is measured by AC calorimeter in the case of dynamic heat capacity?*

The complex dynamic heat capacity $\mathbf{C}_{\rm s}(\omega)$ of a sample can be measured by AC calorimeter in the appropriate frequency range. The heat capacity becomes complex and frequency dependent, when a slow relaxation process occurs in the system.

For measurements of complex heat capacity it is important to measure $\mathrm{Arg}(\mathbf{C}_{\rm eff})$ correctly. The trivial phase lag $-\pi/2$ is not of interest. Consider the phase shift $\varphi_{\rm s}$ between the temperature modulations on the opposite sides of a sample. This phase shift is a sum of two contributions. The first contribution is equal to $\mathrm{Arg}\{1/\mathbf{C}_{\rm s}(\omega)\}$. This contribution to the value of $\varphi_{\rm s}$ is positive. Note, that by definition $\mathbf{C}(\omega)=C'-{\rm i}C''$, where $C''>0$. The second contribution is equal to the phase lag φ_κ, depending on the system thermal conductivity. As follows from Eq. (2), the value φ_κ depends on the parameter $\alpha_{\rm s}=k_{\rm s}d_{\rm s}$, characterizing the thermal length of the sample. This contribution is negative and it tends to minus infinity, when the thickness of the sample and/or modulation frequency are increased. Consequently, it is possible to distinguish these two contributions. Therefore, a peak of $\varphi(T)$ dependence, related to $\mathrm{Im}\mathbf{C}_{\rm s}$, can be measured. On the other hand, the value of calculated thermal conductivity contains two physically different contri-

butions. The first is true thermal conductivity, related to φ_κ. The second is the contribution proportional to $\mathrm{Im}(\mathbf{C}_s)$. In this case, the calculated thermal conductivity should be renamed as *effective thermal conductivity* κ_{eff}, which is equal to the true κ_s, when the sample heat capacity is real-valued. Finally, note that the calculated C_s is the absolute value of the complex $\mathbf{C}_s$. Of course, it is impossible to separate three parameters C_s, $\mathrm{Im}\mathbf{C}_s$, and κ_s, when only two, T_A and φ, are measured. However, in number of interesting cases (near phase transitions) a maximum proportional to C'' can be well-defined on top of the smooth temperature dependence of thermal conductivity, which has no peak, but rather minimum or no anomaly.

2.3. Excess heat capacity and the phase shift at non-reversing melting

Consider a melting transition with the transition enthalpy H, which is smeared in the temperature interval ΔT. Assume that the modulation amplitude T_A is smaller than this interval. In the case of completely reversing melting, the heat $Q \sim \lambda T_A$, absorbed on heating, is the same as released at cooling, where $\lambda = \Delta H/\Delta T$. Then, the excess heat capacity C_{ex}, arising due to reversing melting-crystallization, is real-valued and $C_{ex} \sim \lambda$. If the melting is non-reversing, a part $\varepsilon \cdot Q$ of the heat absorbed on heating is not released on cooling. In this case, the effective non-zero imaginary contribution $\mathrm{Im}\mathbf{C}_{ex} \sim \varepsilon \cdot \lambda/(i\omega)$ to the excess heat capacity appears [10]. This result is in agreement with the calculations for different models discussed in [11]. Actually, the measured value of the excess heat capacity $\mathbf{C}_{ex}(\omega)$ depends on the experimental conditions, such as the underlying heating rate and the thermal history. More over, the measured $\mathrm{Im}\mathbf{C}_{ex}$ cannot tend to infinity, when ω tends to zero, because of the measured signal averaging on a finite frequency interval. This interval depends on the averaging time constant of the apparatus. On the other hand, when the apparatus time constant is not changed the dependency $\mathrm{Im}\mathbf{C}_{ex} \sim 1/\omega$ can be observed. Thus, the complex excess heat capacity can be measured by AC calorimeter in the case of non-reversing cycling at melting transition. Once the complex excess heat capacity is measured, then the positive phase shift due to the imaginary heat capacity appears. This shift is opposite to φ_κ, arising due to the lag in phase related to the thermal conductivity of the sample.

2.4. Material and sample

The PCL sample, received from Prof. G. Groenickx (Catholic University of Leuven, Belgium), was investigated. Polycaprolactone, with the structure $[-(CH_2)_5COO-]_n$, belongs to the aliphatic polyesters. This polymer consists of linear macromolecules with average degree of polymerization n ca. 300. The molecular weight averages were as follows: the number average M_n=34 000, the weight average M_w= 94 000 and the polydispersity M_w/M_n=2.76. At room temperatures, PCL is a semicrystalline polymer with crystallinity, usually, about 40–50%, rigid amorphous fraction 30–40% and the other is mobile amorphous fraction [12]. The crystals in PCL have lamellar structure with narrow size distribution compared to other polymers. Melting of PCL is observed in the temperature range 318–333 K. Glass transition of the mobile amorphous fraction can be observed at 209 K [12,13].

In our experiments, the sample was placed between polished sapphire substrates of the sensor and the heater, without any cuvette. Then, the sample was melted to provide a good thermal contact. The distance between the substrates was fixed in three points by small glass posts. This sandwich was pressed with a thin silk thread. The shape of the melted sample was stable due to the surface tension force. The sample thickness was equal to 0.4 mm, the sample's area S_s was about 6 mm^2 and the sample volume was 2.4×1^{-3} cm^3.

PCL has low thermal conductivity, κ_s ca. 0.4 W/K m, and the heat flux through the sample can produce a noticeable difference of mean temperature at the two sample faces. This temperature difference ΔT_s can be estimated as $\Delta T_s = (P_0 d_s)/(2 S_s \kappa_s)$, $\Delta T_s/P_0 \approx 0.1$ K/mW. Therefore, the average sample temperature equals $T_s = T + \Delta T_s/2$, where T is the temperature measured by the sensor. Most of our experiments were performed at P_0=2.33 mW and ΔT_s ca. 0.2 K.

The time lag in heat transfer through the sample is of very importance, as the melting kinetics is relatively fast. This time lag can be estimated as $\tau_s = (C_s d_s)/(S_s \kappa_s)$. In our experiments, τ_s was ca. 2 s. In our

experiments, the time lag was determined by the averaging time of the lock-in amplifier τ_a=5 s.

3. Results and discussion

3.1. Low temperature measurements

The measurements in the broad temperature range 90–345 K were performed to study the nucleation and vitrification in the sample. In all our experiments the sample was cooled from the melt at 345 K and then heated. Let us compare the experiments at two modulation frequencies f=0.2 and 0.4 Hz. The underlying heating rate q_h was ca. 10 K/min in both cases. The heat-flow amplitude P_0 was equal to 0.58 mW at low frequency and P_0=1.14 mW at 0.4 Hz. Thus the temperature modulation amplitudes were the same at this two frequencies. The amplitude T_A was changed in the range from 0.02 K, at room temperatures, to 0.14 K at low temperatures. Temperature dependences of the effective heat capacity and the phase shift are shown in Fig. 1. The phase shift at the two frequencies is far from zero at room temperature. This means that the sample temperature modulation is not quasi-static. Of course, the effective heat capacities at these frequencies do not coincide. Only at low temperatures the phase shift φ is small, $\varphi\sim-0.1$ rad, and the effective heat capacities for both frequencies are the same. Thus, in the scope of the classical AC calorimetry, the curves are measured non-correctly except low temperatures region near 100 K. So, this curves in the melting region could not be used.

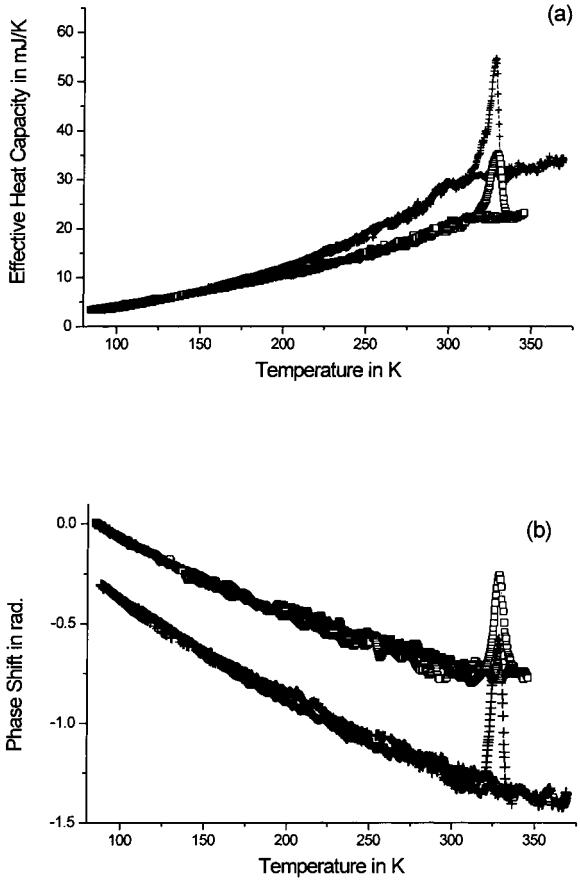

Fig. 1. Temperature dependences of the effective heat capacity (a), and the phase shift (b), for PCL sample of thickness 0.4 mm. The measurements were performed at modulation frequency f=0.2 Hz, heat-flow amplitude P_0=0.58 mW, underlying cooling rate q_c=3 K/min, underlying heating rate q_h=10 K/min (squares), and at f=0.4 Hz, P_0=1.14 mW, q_c=10 K/min, q_h=10 K/min (crosses). The temperature modulation amplitudes were ca. 0.02 K at room temperatures and ca. 0.14 K at low temperatures.

Let us apply our algorithm of calculations to obtain the true heat capacity and the thermal conductivity of the sample. As it is shown in Fig. 2, the calculated temperature dependences of the true sample heat capacity C_s are the same at both frequencies except of the peaks in the melting region. These peaks are dependent on the thermal history. It is remarkable, that different curves in Fig. 1 are converted to a single curve in Fig. 2. This result verifies that the improved AC calorimetry can be applied at high frequencies, when the sample temperature modulation is not quasi-static. The values of the specific heat capacity c_s and the effective thermal conductivity κ_{eff}, are shown in the insert of Fig. 2. The heat capacity dependency is in agreement with the data presented in [12,13], i.e. 1.9–2.0 J/gK in the melt at 350 K and 0.85–0.88 J/gK in the rigid state at 160 K. At frequencies higher than 1 Hz the measured values of heat capacity were larger than the right values, and were increased with frequency. The same effect was observed on sapphire samples at f>10 Hz. The higher the sample thermal conductivity, the higher the frequency limit of the applicability of these calculations. This is due to the effect of cross terms in Eq. (2) and of the heat-leakage into the thermocouple wires. These effects can be taken into account in the second-order approximation.

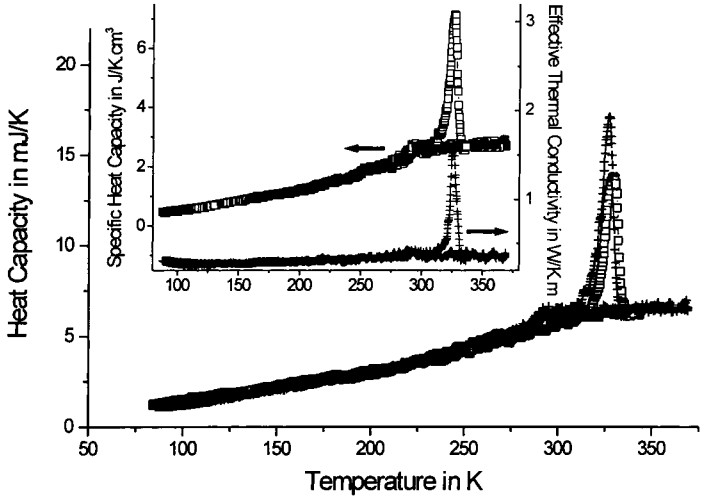

Fig. 2. Temperature dependences of the dynamic heat capacity of PCL sample at modulation frequencies 0.2 Hz (squares) and 0.4 Hz (crosses) at the same conditions as in Fig. 1. The temperature dependences of the specific heat capacity (squares) and the effective thermal conductivity (crosses) at modulation frequency 0.4 Hz are shown in the insert.

Note, that in the melting region, the peaks of the temperature dependences of the phase shift are of positive sign, Fig. 1. Consequently, these peaks are related to the imaginary part of the sample heat capacity, resulting from non-reversing melting. On the contrary, the reversing melting, should cause the negative phase shift. Of course, no peaks in $\varphi(T)$ and $C_s(T)$ dependences were observed at cooling because crystallization is not modulated due to supercooling.

The heating and cooling curves were reproducible. No hysteresis was observed at temperatures below 250 K. A well defined step in the $C_s(T)$ dependence at ca. 290 K is observed. It can be explained by the fast nucleation and crystallization, which takes place in the sample at ca. 290 K. The result is independent on cooling rate, at least when $q_c \leq 10$ K/min. The fast nucleation and crystallization can be attributed to the fact that a number of heterogenities with good nucleating abilities persist in the sample. The analogous fast crystallization was observed in [12] for the sample with a number of heterogenities.

The quasi-isothermal relaxation of the effective heat capacity and the phase shift for PCL at crystallization, is shown in Fig. 3. The measurements were performed at modulation frequency 0.5 Hz, heat-flow amplitude 9.34 mW, modulation amplitude ca. 0.1 K and at 318 K after the sample was cooled from the melt with the cooling rate ca. 5 K/min. The heat capacity decreases at crystallization and the phase shift decreases also. The rate of crystallization can be described by the time of half relaxation, $t_{1/2}$. The value of $t_{1/2}$ equals ca. 450 s at 318 K. This value of relaxation time is in agreement with the results, $t_{1/2}$=190 s at 316 K and $t_{1/2}$=690 s at 320 K, presented in [12] for the sample with comparatively large number of heterogenities. The analogous relaxation at 311 K is shown in the insert of Fig. 3. In this case the rate of crystallization is by an order of magnitude faster, $t_{1/2} \sim 40$ s at 311 K.

3.2. Thermal history

The melting kinetics depends on thermal history. Therefore reproducible sample preparation is necessary before studying melting kinetics. From preliminary experiments we found out that the sample can be prepared as follows: 5 min nucleation at 318 K, after fast cooling from the melt, then crystals growth at $T_{cr} \approx 329$ K, after fast heating. In this way it was possible to grow crystals reproducibly and relatively fast, which show a melting temperature $T_m \approx 334.5$ K and relatively narrow crystal's thickness distribution, as shown in Fig. 4. Note, that the peaks of quasi-isothermal relaxation at 332.6 K and at 334.5 K are higher than the peak at 330.7 K.

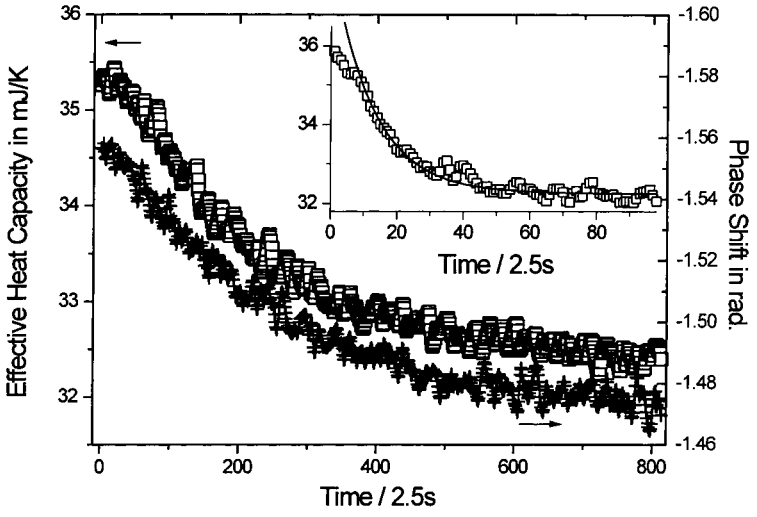

Fig. 3. Quasi-isothermal relaxation of the effective heat capacity (squares) and the phase shift (crosses) for PCL at crystallization. The measurements were performed at modulation frequency 0.5 Hz, heat-flow amplitude 9.34 mW, modulation amplitude ca. 0.1 K and at 318 K after sample cooling from the melt with the underlying cooling rate ca. 5 K/min. The analogous relaxation at 311 K is shown in the insert.

3.3. Stationary level and zero crystallinity line

Before studying quasi-isothermal relaxation of excess heat capacity, it was necessary to determine stationary level of dynamic heat capacity, i.e. the level, to which the time dependence $\mathbf{C}_s(t)$ tends at infinity. Of course, this level depends on thermal history. But it was possible to prepare samples reproducible. The question arises if this level depend on modulation frequency and/or temperature modulation amplitude. Consider the quasi-isothermal relaxation of the dynamic heat capacity and the effective thermal conductivity to the stationary levels at 331.3 K, shown in Fig. 5. The measurements were performed at modulation frequency 0.2 Hz, heat-flow amplitude 2.33 mW and modulation amplitude ca. 0.1 K. After reaching stationary level frequency was changed between 0.1 and 1 Hz. As shown in Fig. 5, the stationary levels are independent of frequency in this range. It appears, that after 15 min relaxation the values of the stationary levels of the heat capacity and the effective thermal conductivity are close to the levels of zero crystallinity. These zero-crystallinity levels were measured, when cooling from the melt. The stationary and zero-crystallinity levels are close to each other, when the temperature is sufficiently high and no appreciable crystallization occurs. This result was proved at different amplitudes T_A in the range 0.005–0.2 K, frequencies in the range 0.1–1Hz, temperatures 329, 330, 331, and 338 K, and different thermal histories. Indeed, the stationary levels of the phase shift and of the effective heat capacity are strongly frequency dependent, as shown in Fig. 6. On the contrary, the stationary levels of the true heat capacity and thermal conductivity obtained from Eqs. (2) and (4) are frequency independent.

3.4. Melting kinetics

Relaxation of the dynamic heat capacity of semi-crystalline polymers can often be observed after step heating of the sample in the melting region [9]. Because of the large time constants in TMDSC, which are of the order of minutes, it is not possible to follow the relaxation process from the very beginning. With the faster AC calorimeter, τ_a ca. 1 s, it should be possible to follow the relaxation immediately after reaching the new temperature. The quasi-isothermal relaxation of the excess heat capacity is relatively fast at short times and it should be proved that the apparatus time lag is of no importance. In our case, the time lag is determined by the averaging time of the lock-in amplifier. From the quasi-isothermal relaxation of the effective heat capacity at different time constants,

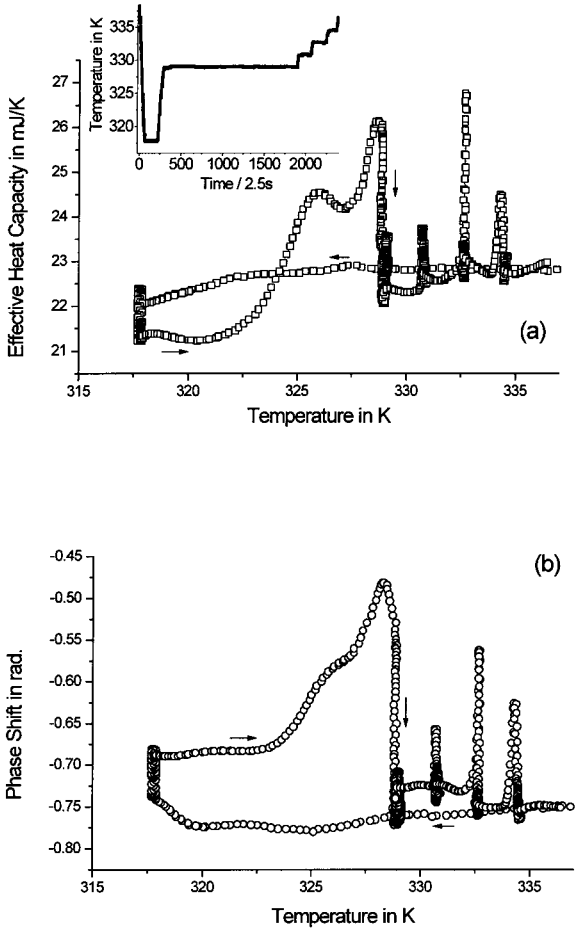

Fig. 4. Temperature dependences of the effective heat capacity (a), and the phase shift (b) for PCL at modulation frequency 0.2 Hz, heat-flow amplitude 2.33 mW and T_A ca. 0.1 K. The measurements were performed at cooling from the melt with the underlying rate ca. 8 K/min, 5 min pause at 317.5 K for the nucleation and 1 h pause at 329 K for crystals growth. Then the temperature was changed in steps of 1.9 K every 5 min. The temperature vs time dependence is shown in the insert.

shown in Fig. 7, it can be concluded that the influence of the apparatus time lag is negligible for τ_a<10 s. Therefore all experiments were performed at $\tau_a \leq 5$ s.

It was found, that the quasi-isothermal relaxation of the excess heat capacity was independent of the temperature-modulation amplitude in the range 0.05–0.2 K, as shown in Fig. 8. Finally, to describe the quasi-isothermal relaxation of the excess heat capacity as a function of time, one should answer the following question: Where is the zero point of the

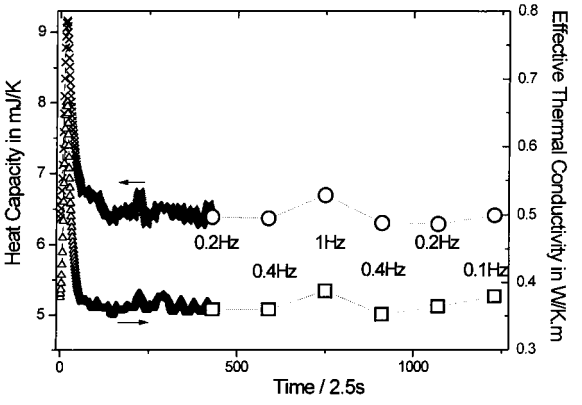

Fig. 5. Quasi-isothermal relaxation of the dynamic heat capacity (crosses) and the effective thermal conductivity (triangles) to the stationary levels for PCL at 331.3 K after step-heating in the melting region. The measurements were performed at modulation frequency 0.2 Hz, heat-flow amplitude 2.33 mW and modulation amplitude ca. 0.1 K. After 15 min of relaxation the values of the stationary levels were measured at different frequencies for every 5 min (circles and squares). The sample was cooled from the melt to 311 K in steps of 1.9 K for every 15 min, then heated in steps of 1.9 K for every 30 min.

time scale? The relaxation was measured at a fixed temperature after step-heating. In the experiment the step was not absolutely sharp. It took about 30 s to change the temperature by 1.9 K. The signal started to vary with an appreciable delay after temperature variation. The heat capacity started to noticeably

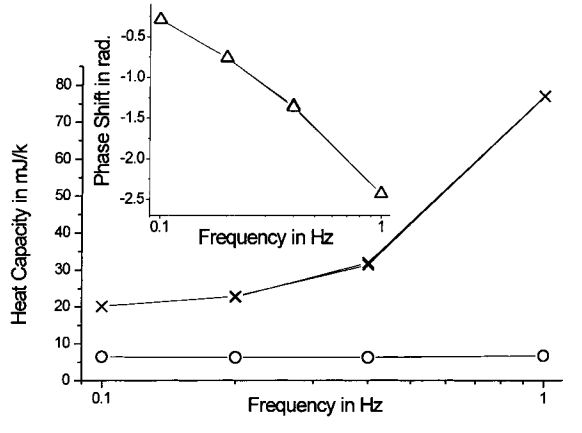

Fig. 6. Frequency dependences of the stationary levels of the effective heat capacity (crosses), the heat capacity (circles) and the phase shift (triangles) for PCL sample at the same conditions as in Fig. 5.

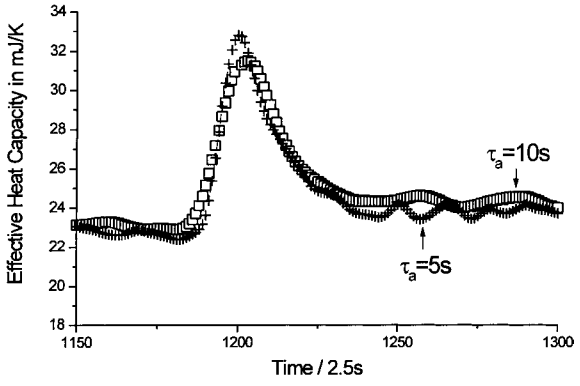

Fig. 7. Quasi-isothermal relaxation of the effective heat capacity for PCL after step-heating in the melting region at 329.5 K. The sample was cooled from the melt to 311 K with the underlying cooling rate ca. 3 K/min, then heated in steps of 1.9 K for every 5 min. The measurements were performed at modulation frequency 0.2 Hz, heat-flow amplitude 2.33 mW, modulation amplitude ca. 0.1 K, and at different time constants of the lock-in amplifier: τ_a=5 s (crosses) and 10 s (squares).

increase after the temperature came to a constant level. This point was chosen as zero of the time scale. From this moment the heat capacity increased during ca. 30 s and then relaxed. The important point is that the melting process began not immediately after the temperature change, but with an appreciable lag. This lag can be attributed neither to that of the apparatus, τ_a=5 s, nor to the lag in heat transfer through the sample, $\tau_s \approx 2$ s. Therefore, an appreciable time is required to initiate the melting process. It can be assumed, that the melting in this polymer is related to an activation process. It appears, the melting kinetics can be described by the following equation:

$$C_s(t) = C_b + C_{ex} \exp(-t/\tau_0)\,[1 - \exp(-bt^n)], \quad (5)$$

where C_b – base-line heat capacity, C_{ex} – excess heat capacity, τ_0 – relaxation time of the melting process, b and n the parameters of the stretched exponent. The stretched exponent describes the initiating of the melting process. The decay of the melting is described by the exponent with time constant τ_0. As shown in Fig. 8, the experimental curves can be approximated by this time dependence at reasonable parameters. It is noteworthy, that the attempts to approximate the dynamic heat capacity relaxation by two simple exponents, $\exp(-t/\tau_2)$ ($[1-\exp(-t/\tau_1)]$, had no success.

The tails of the relaxation curves can be approximated by the only exponent. It was found, that the effective heat capacity and the phase shift decay with the same rate, as shown in Fig. 9. This means, that the decay processes of the real and the imaginary parts of the excess heat capacity are described by the same

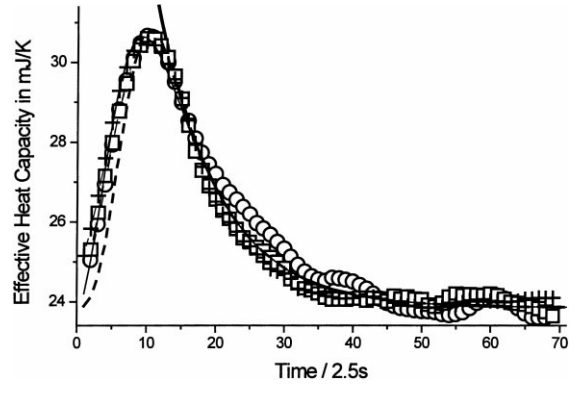

Fig. 8. Time dependences of the quasi-isothermal effective heat capacity for PCL at different amplitudes T_A ca. 0.05 K (squares), 0.1 K (circles), 0.2 K (crosses) at the same conditions as in Fig. 7 with τ_a=5 s. The curves are normalized to the maximum of the curve with T_A=0.05 K. The curves can be approximated by the following time dependence: $23.85+27\exp(-t/\tau_0)[1-\exp(-bt^n)]$, where τ_0=23 s and n can be in the range from 2 to 3, with b=0.0015 at n=3 (dash line) and b=0.014 at n=2 (thin line). The tails of the curves can be approximated by the only exponent $23.85+27\exp(-t/\tau_0)$ (thick line).

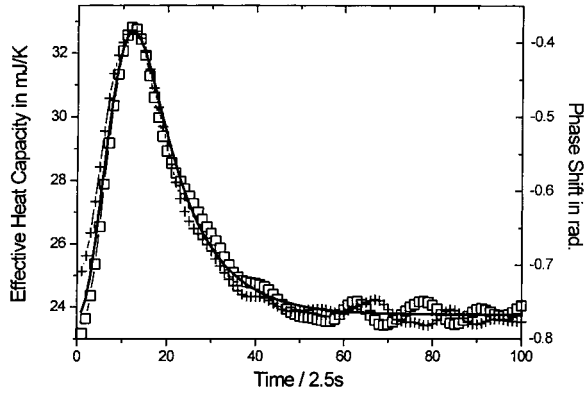

Fig. 9. Quasi-isothermal relaxation of the effective heat capacity (squares) and the phase shift (crosses) for PCL after step-heating in the melting region at the same conditions as in Fig. 7 with τ_a=5 s. The curves was approximated by the same time dependence as in Fig. 8, with τ_0=25 s, n=2.4 and b=0.003 (thick line).

exponent $\exp(-t/\tau_0)$ at the same temperature and frequency. This can be explained as follows. Denote the total volume V_{cr} of the crystals in the sample. Assume that this volume decreases exponentially in the isothermal melting process after a small heating step. Of course, we consider the case, when only a small fraction of the crystals, with the same parameters, is melted. If the value of $\mathrm{Re}\mathbf{C}_{ex}$ is related to the reversing melting and $\mathrm{Im}\mathbf{C}_{ex}$ is related to the non-reversing melting, then $\mathrm{Re}\mathbf{C}_{ex} \sim V_{cr}$ and $\mathrm{Im}\mathbf{C}_{ex} \sim \partial V_{cr}/\partial t$ at constant temperature and frequency. Thus, the following relation can be written $\partial/\partial t(\mathrm{Re}\mathbf{C}_{ex}) \sim \mathrm{Im}\mathbf{C}_{ex} \sim \exp(-t/\tau_0)$ and $\mathrm{Re}\mathbf{C}_{ex} \sim \exp(-t/\tau_0)$ for the excess heat capacity decay. Therefore, it is sufficient to investigate the relaxation of $\mathbf{C}_{eff}$ without calculation of $\mathbf{C}_s$. As shown in Fig. 9, the dependences $C_{eff}(t)$ and $\varphi(t)$ can be approximated by the relation (5) with reasonable parameters. It was found, that these parameters are independent on modulation amplitude and frequency in the range 0.1–1 Hz, but they are temperature and thermal-history dependent.

The temperature dependences $C_{ex}(T)$ and $\tau_0(T)$ was investigated at the following three types of thermal histories. At first thermal treatment, the sample was cooled from the melt below 310 K and heated to 325 K with the heating-cooling rate ca. 5 K/min, then measurements were performed in steps of 1.9 K for every 5 min. In the second case, the sample was cooled from the melt to 311 K with the underlying cooling rate ca. 3 K/min, then heated in steps of 1.9 K for every 5 min, and crystals growth were performed at 329.5 K during 30 min. The third thermal history is the same as in Fig. 4. This thermal treatment provides the most large crystals and with the most narrow crystal's thickness distribution. In this case, the most slow relaxation is observed, as shown in Fig. 10. Thus, the third thermal treatment provides comparatively large and perfect crystals, with high τ_0 and $(T_m)_{max}$. On the other hand, the crystallinity was relatively small, in this case. The maximal value of the excess heat capacity $(C_{ex})_{max}$ was ca. 2.5 mJ/K at 332.6 K. This is two times smaller than $(C_{ex})_{max}$ at 329.5 K, in the case of the second-type thermal history. Finally, a lot of small, imperfect crystals was in the sample after the first-type thermal treatment: $(C_{ex})_{max}$ was ca. 10 mJ/K at 326 K, with relatively small τ_0 and $(T_m)_{max}$. These results are in agreement with conclusions of Section 3.2.

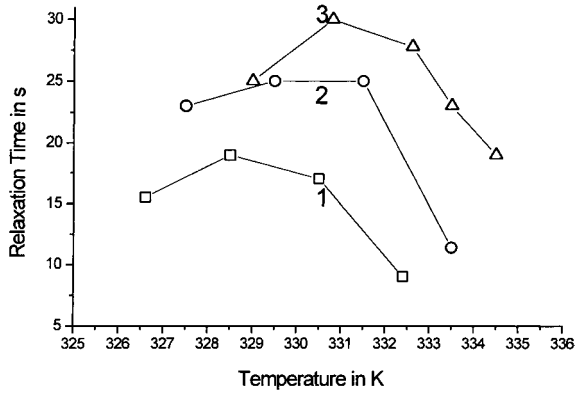

Fig. 10. Temperature dependences of the relaxation time-constant τ_0 of the quasi-isothermal dynamic heat capacity of PCL at three types of the thermal histories: 1 – the sample was cooled from the melt below 310 K and heated to 325 K with the heating-cooling rate ca. 5 K/min, then measurements were performed in steps of 1.9 K for every 5 min (squares), 2 – the sample was cooled from the melt to 311 K with the rate ca. 3 K/min, then heated in steps of 1.9 K for every 5 min except 30 min pause at 329.5 K (circles), and 3 – the temperature variation was the same as in Fig. 4 (triangles).

4. Conclusions

The new capabilities of AC calorimeter, when working at frequencies above the classical limit were demonstrated. The width of appropriate frequency range of the classical AC calorimetry was substantially enlarged. It was shown, that the advanced AC calorimetry can be successfully applied for studying of the dynamic heat capacity of polymers at frequencies ca. 1 Hz. Therefore, the apparatus time lag can be as small as ca. 1 s. The time lag in heat transfer through the sample was also small, ca. 2 s. It was shown, that simultaneous determination of heat capacity and thermal conductivity is possible, when phase and amplitude of the sample temperature modulation are measured.

The advanced AC technique was applied for investigation of the melting kinetics in polycaprolactone. The following new information about the melting kinetics of polycaprolactone was obtained. It was found, that the stationary level of the dynamic heat capacity is independent of frequency in the range 0.1–1 Hz. It appears, that the stationary levels of the heat capacity and the effective thermal conductivity coincide with the levels of zero crystallinity, at least at

sufficiently high temperatures, above 329 K. This result was proved at temperature-modulation amplitudes in the range 0.005–0.2 K, and at different thermal histories.

It appears, that the appreciable time period is required to initiate the melting process after step-heating. Thus, melting in polycaprolactone is related to an activation process. The activation of the melting process is described by a stretched exponent and the decay of the melting by only one exponent at short times until 4 min. The dependencies of the exponent's parameters on temperature and thermal history were investigated.

Acknowledgements

The financial support of the European Commission, grant number IC15CT96-0821, is gratefully acknowledged.

References

[1] P.F. Sullivan, G. Seidel, Phys. Rev. 173 (1968) 679.
[2] P. Handler, D.E. Mapother, M. Rayl, Phys. Rev. Lett. 19 (1967) 356.
[3] M.B. Salamon, Phys. Rev. B 2 (1970) 214.
[4] I. Hatta, A. Ikushima, J. Phys. Chem. Solids 34 (1973) 57.
[5] Y.A. Kraftmakher, Compendium of Thermophysical Property Measurement Methods, vol. 1, Plenum press, New York, 1984, p. 591.
[6] B. Wunderlich, WWW address: http:// www.utk.edu/~athas/courses.
[7] K. Ema, H. Yao, Thermochimica Acta 304–305 (1997) 157.
[8] M. Reading, Trend Polym. Sci. 8 (1993) 248.
[9] C. Schick, M. Merzlyakov, B. Wunderlich, Polym. Bull. 40 (1998) 297.
[10] A.A. Minakov, Yu.V. Bugoslavsky, C. Schick, Thermochim. Acta 317 (1998) 117.
[11] J.E.K. Schawe, E. Bergmann, Thermochim. Acta 304–305 (1997) 179.
[12] P. Skoglund, A. Fransson, J. Appl. Polym. Sci. 61 (1996) 2455.
[13] B. Wunderlich, WWW address: http:// www.utk.edu/~athas/databank.